Title

Concurrent measurement of strain and chemical reaction rates in a calcite grain pack undergoing pressure solution: Evidence for surface-reaction controlled dissolution

Authors

Lisabeth, Harrison
DePaolo, Donald J
Pester, Nicholas J
et al.

Publication Date

2024-11-01

DOI

10.1016/j.gca.2024.09.018

Geochimica et Cosmochimica Acta 385 (2024) 184–198

Contents lists available at ScienceDirect

Geochimica et Cosmochimica Acta

journal homepage: www.elsevier.com/locate/gca

Concurrent measurement of strain and chemical reaction rates in a calcite grain pack undergoing pressure solution: Evidence for surface-reaction controlled dissolution

Harrison Lisabeth *, Donald J. DePaolo, Nicholas J. Pester, John N. Christensen

Energy Geosciences Division, Lawrence Berkeley National Laboratory, Berkeley, CA 94720, United States

ARTICLE INFO

Associate editor: Matthew S. Fantle

Keywords:
Carbonate
Chemical-mechanical processes
Calcite
Isotope geochemistry
Pressure solution
Trace element geochemistry
Experimental rock chemo-mechanics
Fluid-rock interaction

ABSTRACT

Pressure solution is inferred to be a significant contributor to sediment compaction and lithification, especially in carbonate sediments. For a sediment deforming primarily by pressure solution, the compaction rate should be directly related to the rate of calcite dissolution, transport along grain contacts, and calcite reprecipitation. Previous experimental work has shown that there is evidence that deformation in wet calcite grain packs is consistent with control by pressure solution, but considerable ambiguity remains regarding the rate limiting mechanism. We present the results of laboratory compaction experiments designed to directly measure calcite dissolution and precipitation rates (recrystallization rates) concurrently with strain rate to test whether measured rates are consistent with predicted rates both in absolute magnitude and time evolution. Recrystallization rates are measured using trace element chemistry (Sr/Ca, Mg/Ca) and isotopes ($^{87}Sr/^{86}Sr$) of fluids flowing slowly through a compacting grain pack as it is being triaxially compressed. Imaging techniques are used to characterize the grain contacts and strain effects in the post-experiment grain pack. Our data show that calcite recrystallization rates calculated from all three geochemical parameters are in approximate agreement and that the rates closely track strain rate. The geochemically inferred rates are close to predicted rates in absolute magnitude. Uncertainty in grain contact dimensions makes distinguishing between surface reaction control and diffusion control difficult. Measured reaction rates decrease faster than predicted from standard pressure solution creep flow laws. This inconsistency may indicate that calcite dissolution rates at grain contacts are more complex, and more time-dependent, than suggested by geometric models designed to predict grain contact stresses.

1. Introduction

The carbonate mineral calcite is one of the most common constituents of sedimentary rocks in the Earth's crust. The compaction and diagenesis of calcite-bearing sediments control the porosity, permeability and strength of these sedimentary rocks. Understanding the mechanisms of diagenesis is the key to producing reliable predictive models of the properties and behavior of carbonate hydrocarbon reservoirs, aquifers, caprocks for geological storage and fault damage zones.

Although substantial progress has been made towards a mechanistic understanding of the diagenesis of carbonate sediments, considerable ambiguity remains as to the relative contributions of several mechanisms. Porosity reduction can be caused by both mechanical processes, such as grain comminution and rearrangement, and chemical processes, such as authigenic carbonate precipitation. It is well known that at shallow burial depths, porosity loss is primarily driven by mechanical compaction (Scholle and Halley, 1985). The primary mechanism of this rapid initial compaction appears to be grain rearrangement facilitated by frictional sliding (Renard et al., 2001). At elevated deviatoric stresses, shear enhanced compaction can lead to further reductions in porosity (Zhu et al., 2010; Vajdova et al., 2010) but this process itself can be sensitive to fluid chemistry (Lisabeth and Zhu, 2015) and other chemical mechanisms play a central role at greater depths.

The two main chemically-coupled compaction mechanisms at play in carbonate sediments are pressure solution and subcritical cracking. Pressure solution is a process by which mass is moved from stressed grain contacts to unstressed adjacent pore walls (Weyl, 1959; Rutter, 1983). Subcritical cracking is the slow growth of cracks through chemical weakening of crack tips (Atkinson, 1984), which can result in grain comminution, rearrangement and porosity reduction. A thorough

* Corresponding author.
E-mail address: hlisabeth@lbl.gov (H. Lisabeth).

https://doi.org/10.1016/j.gca.2024.09.018
Received 19 June 2022; Accepted 13 September 2024
Available online 16 September 2024

review of the observational and experimental literature on this subject is presented by Croizé et al. (2013), but for the sake of clarity, we will outline some outstanding questions.

Pressure solution creep has been suggested as an important mechanism for compaction in sedimentary basins (Rutter, 1983) and for healing of faults (Hickman and Evans, 1995). The driver of pressure solution is stress-induced, elevated solubility at grain contacts leading to diffusion of dissolved species away from contacts and, in a closed system, local reprecipitation in slightly supersaturated pore fluid (Lehner, 1990; Spiers and Schutjens, 1990). In an open system, dissolved species may be advected away. Experimental studies of pressure solution in carbonate samples employing both oedometers and indenters at a range of grain sizes, stresses, temperatures and pore fluid chemistries have yielded inconsistent evidence for rate limiting steps; for instance, the early work of Baker et al. (1982) suggests surface reaction limitation based on the salinity dependence of recrystallization, while several studies (Spiers et al., 1990; Spiers and Schutjens, 1990; Zhang et al., 2002; Croize et al., 2010) conclude diffusion limitation on the basis of the grain size dependence of creep rates. Diffusion-limited creep has become something of a consensus in the pressure solution literature; however, evidence for other rate limiting steps persists in the literature. Zhang and Spiers (2005a) report a reduction in creep upon the addition of Mg to pore fluids and an increase in creep with the addition of NaCl. Systematic study of the effect of phosphate in solution resulted in a creep rate consistent with reductions of calcite precipitation kinetics predicted due to the presence of phosphate (Jonasson et al., 1996; Zhang and Spiers, 2005b). Additionally, experiments at low pH exhibit evidence for both pressure solution and fracturing operating concurrently (Le Guen et al., 2007; Liteanu and Spiers, 2009). In limestones, even where pressure solution has been shown to be the likely mechanism, it is unclear whether dissolution is transport controlled or surface reaction controlled (e.g. Spiers and Schutjens, 1990). It is common for constitutive relations describing relaxation processes like compaction creep to be agnostic to any specific mechanism due to the range of length- and timescales for concurrent processes (Snieder et al., 2017). However, because pressure solution entails successive dissolution and reprecipitation, pressure solution should impart a characteristic trace geochemical and isotopic signature to pore fluid governed by the fractionation of the respective elements and isotopes.

Much of the ambiguity concerning deformation due to pressure solution stems from the ambiguous relationship between reaction rates and strain rates. Flow laws such as those discussed in Zhang et al. (2010) and related studies ultimately relate the ratio of reaction rates to strain rates via the ratio of contact area to grain diameter, which is model-dependent. In addition, the formulation of surface reaction rate remains uncertain due to ambiguity about the properties of intergranular films and to general uncertainties associated with the relationship of calcite dissolution rate to departure from equilibrium, especially when the solid surface structure may be complicated. To begin to address this ambiguity, we have run a series of flow-through calcite compaction experiments designed to quantitatively measure the dissolution and precipitation rates of calcite using three different geochemical indicators. In this paper, we first describe the methodology, then report the measured geochemical data and concurrently measured mechanical data. We present a framework to analyze the pore fluid chemistry to recover bulk calcite reaction rates and finally discuss the results in the context of prevailing models and theories.

2. Experimental details

An extensive geochemical and isotopic assay of several potential calcite materials was made to determine the ideal material for experiments. The sample material was monomineralic calcite derived from three different sources chosen to maximize contrasts in chemical properties and allow for optimal application of our techniques (Supplementary Material, Part 1). The calcite varieties were given the informal names of "Water Treatment Marble (WTM)," "Iceland Spar (MXS)," and "Junkyard marble (JYM)." Each is pure low-Mg calcite. The Iceland Spar is optical grade calcite from Mexico obtained from Ward's Science and was used to produce starting solutions. WTM is granular calcite marble from Georgia used for water treatment (calcite filtration media Z, Pure Water Site). JYM is from a discarded marble weighing table. Two of the calcite samples (JYM and WTM) were used as column material, and were chosen for their Sr/Ca, Mg/Ca and $^{87}Sr/^{86}Sr$ ratios (Table 1), so that appropriate contrasts between the starting fluids and solids in the experiments would allow for accurate geochemical measurement of calcite reaction rates.

Calcite grains are rhombic with significant surface fines prior to cleaning. In Experiment 1, the JYM calcite grain size was constrained only to < 120 μm. It was also not ultrasonically cleaned prior to the experiment and was coated with a small amount of fine material (Supplementary Fig. S2b). In Experiment 3 the crushed WTM calcite was sieved to a grain size between 90 and 212 μm and rinsed several times ultrasonically in ethanol. After cleaning, calcite surfaces appeared free of fines (Supplementary Fig. S2a).

The calcite substrate material was weighed out and assembled into the loading column of a triaxial pressure vessel plumbed for fluid flow and capable of independent control of confining and axial stress. Detailed specification of the pressure vessel can be found in Voltolini et al. (2017). Axial pressure, confining pressure and fluid flow are all provided using computer controlled high pressure pumps (ISCO 500D) and measured using calibrated transducers (Honeywell LM-DV, 0.5 % accuracy). The flow rate, total volume and pressure from each pump are logged continuously during experiments. The downstream side of the pore pressure system was connected to an autosampler to facilitate serial pore fluid sampling. Axial stress is calculated using the axial pressure and sample diameter and the confining and pore pressures are measured using the transducers in the pumps. Axial deformation was measured using an LVDT affixed to the loading piston. As the granular sample was significantly more compliant than the loading system itself and the stresses remained low, the load column deformation was neglected. A PTFE heat shrink jacket was used to separate the granular calcite from the confining medium and the grain pack was sandwiched between 0.2-μm PTFE filters to prevent grains from entering the pore fluid lines. The sample was agitated mechanically and tamped down until the grain pack was flat and level. 2.7 g of calcite was used and uncompacted samples have an initial porosity of 48 %. Porosity was measured using the sample geometry and mass assuming the solid was 100 % calcite. Once the vessel was sealed it was put into a forced air oven (VWR Gravity Convection Incubator) and confining pressure was applied using water as a confining medium and pore fluid lines connected. Temperature inside the oven was monitored throughout the experiment (HoboLogger

Table 1
Chemical and isotopic composition of calcite samples.

	JYM	WTM	MXS
Ca wt %	38.13	37.85	39.29
Mg, wt %	0.12	0.58	0.11
Fe, wt %	0.03	0.05	ND
Mn, ppm	17.7	131	184
Li, ppm	1.78	0.70	0.43
Al, ppm	27.4	30.0	17.7
P, ppm	16.7	346	18.0
K, ppm	113	166	71
Zn, ppm	10.60	16.74	5.40
Sr, ppm	196	1115	337
Ba, ppm	2.38	2.33	0.13
Cu, ppm	24.4	6.17	ND
Cr, ppm	0.07	0.08	1.09
Pb, ppm	0.54	1.42	0.01
Sr/Ca (mmol/mol)	0.235	1.348	0.392
Mg/Ca (mmol/mol)	5.275	25.343	4.526
$^{87}Sr/^{86}Sr$	0.70919	0.70847	0.70957

MX1101). Pore fluid for flow (starting solution) was carefully equilibrated with the MXS calcite at 1 atmosphere pressure and room temperature (Supplementary Figure S1) to minimize net dissolution during the experiments. A schematic and photo of the experimental apparatus is presented in Fig. 1.

We ran one 60-hour (Experiment1) and one 300 + hour-long (Experiment 3) triaxial compaction creep experiments on granular calcite while monitoring stress, strain, temperature and fluid chemistry. Experiment 2 was designed for X-ray analysis at the Advanced Light Source, was not fully characterized, and is described in the Supplementary Material. Experiment 1 was conducted at a confining pressure of 5 MPa and an axial stress of 7 MPa while Experiment 3 was conducted at confining pressure of 10 MPa and axial stress of 15 MPa, roughly corresponding to depths of 100 and 500 m. All experiments were run at 23 °C.

Confining pressure and axial pressure were raised to experimental conditions at a rate of 0.2 MPa/min simultaneously to ensure an initial hydrostatic stress state. The sample was then allowed to equilibrate for several hours. Pore fluid was then flushed through the system at a rate of 5 mL/min until the core was saturated and an initial fluid sample of 6 mL was collected. The fluid flow rate was then reduced to 0.01 mL/min. The axial stress was then increased to experimental conditions immediately and held constant throughout the experiment. Fluid samples were taken continuously every 10 h, resulting in sequential 6 mL fluid samples. Blank fluid samples were taken directly from the pump throughout the duration of the test to monitor any possible evolution of the starting fluid. At the conclusion of the test, the system was depressurized and the sample removed for further analysis.

3. Results

3.1. Mechanical data

The mechanical behavior of the samples is consistent with typical creep compaction curves, initial fast compaction and deceleration as the experiment progresses; although, it should be mentioned there are several aspects of our experiments that deviate from typical creep compaction experiments. First, compaction experiments are typically performed odeometrically, with rigid walls. Our sample was allowed to expand laterally; this complicated the calculation of volumetric strain from axial strain, because we do not measure lateral strain directly. We calculate volumetric strain assuming a lateral expansion one tenth of the axial contraction. This assumption is derived from a complementary experiment run while performing *in situ* tomography (Supplementary Material, Part 3). Second, we do not hold pore pressure constant, but rather flow rate. As a result of changes in the pore network, the pore pressure increases during the experiment, leading to a reduction in effective stresses over time; therefore, ours are not constant stress experiments (Supplementary Figure S7).

3.2. Chemical and isotopic data

We measure Ca, Mg, Sr and Sr isotopes in our effluent pore fluid. Ca concentrations are used to evaluate the bulk saturation state of our experiments. Trace element and isotopic ratios are used to evaluate in-situ reactions. The concentrations of Ca, Sr and Mg in the experimental solutions and starting carbonate minerals were measured using Inductively Coupled Plasma Optical Emission Spectroscopy (ICP-OES). Sr isotope analyses for $^{87}Sr/^{86}Sr$ ratios were conducted in the labs of the Center for Isotope Geochemistry at Lawrence Berkeley National Lab and on the campus of the University of California, Berkeley using a Triton multi-collector magnetic sector thermal ionization mass spectrometer (ThermoFisher Scientific). Additional analytical details are provided in Supplementary Material, Part 1. Time series chemical data from Experiments 1 and 3 are presented in Tables 2 and 3 and illustrated in Fig. 3.

Dissolved Ca in the effluent from both experiments varied during the experiments but was mostly within ± 10 % of the pre-saturated starting

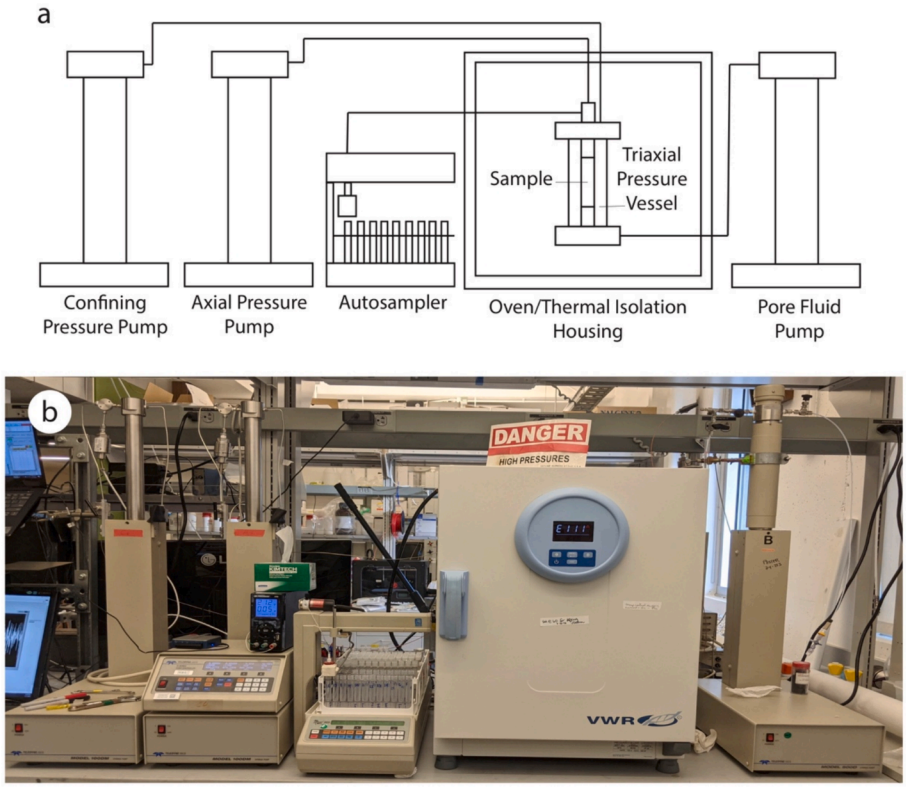

Fig. 1. Experimental apparatus. a) a schematic and b) photograph of the experimental setup.

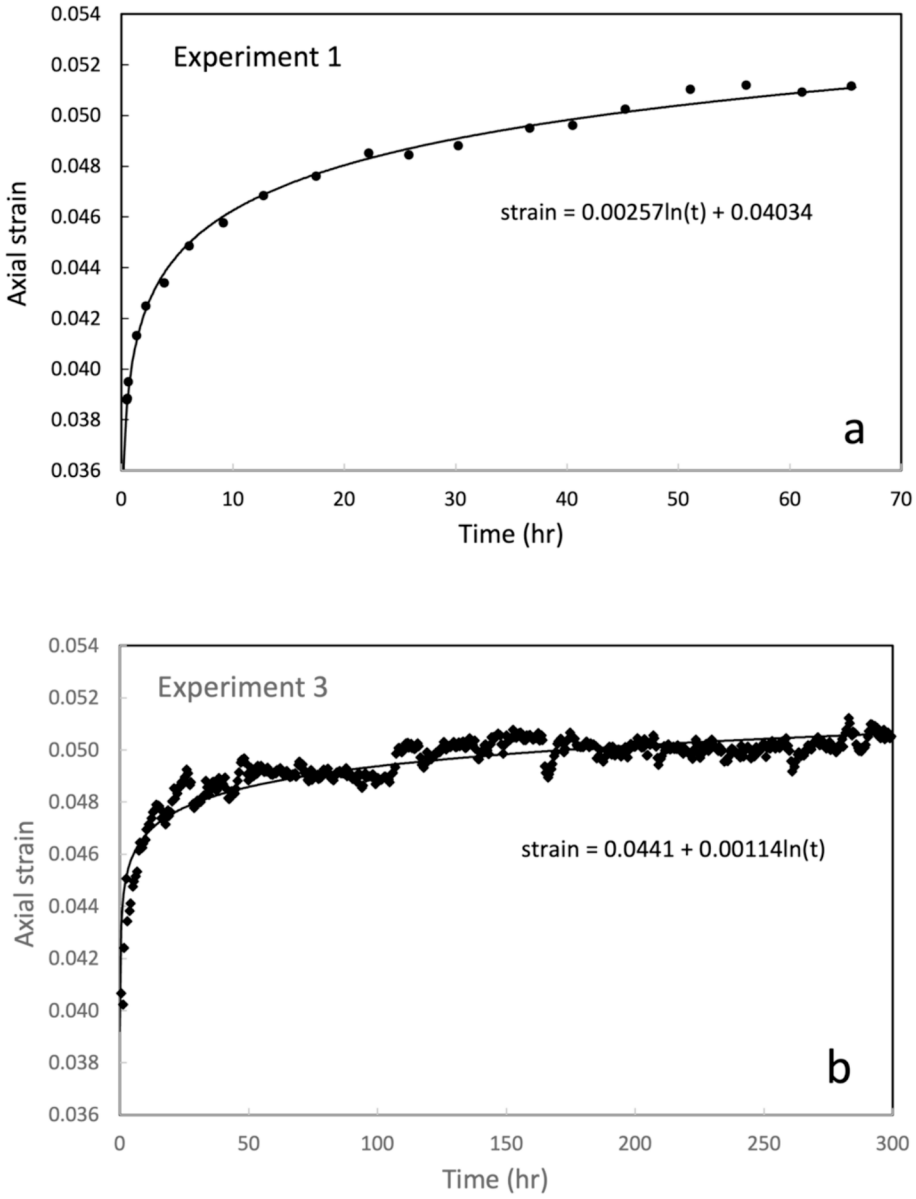

Fig. 2. Details of axial strain vs time for (a) Experiment1 and (b) Experiment 3. The data can be fit with logarithmic functions, giving a value for strain rate of 0.00257/t for Experiment 1 and 0.00114/t for Experiment 3, with time in hours. Mechanical data have been down-sampled for clarity.

solution (Supplementary Figure S10). The Ca concentration variations reflect processes in the column because samples taken from the feed solution reservoir during Experiment 3 remained constant within analytical uncertainty (±3%). The Ca concentration measurements suggest that reaction with the calcite grains in the core are modifying the saturation state of the fluid, but we do not have accompanying data on pH and DIC to evaluate directly whether the fluid was out of equilibrium with calcite, because the effluent is exposed to air while it is accumulating. It is important to note that calcite solubility increases with pressure, and our starting solutions would have been slightly undersaturated at the elevated pressures of our experiments. The effluent Ca values in Experiment 3 are nearly all higher than the source fluid over the first 250 hrs (+5.5 % average), confirming that the starting solution was slightly undersaturated with respect to the bulk calcite grains in the pack. The Ca concentration variations in Experiment 1 are less systematic and smaller than in Experiment 3. Temperature fluctuated in both experiments (e.g. Supplementary Figure S7). An increase in temperature of 3 °C could, for example, cause a 5 % decrease in the equilibrium fluid Ca concentration, within range of the fluctuations we measure.

Both Sr/Ca and Mg/Ca of the effluent start out 10 to 25 times higher than the values for the starting solution and then decrease and approach those of the starting solution (Fig. 3a, b). In analogous fashion, in the initial stages of Experiment 3, the effluent $^{87}Sr/^{86}Sr$ ratio is shifted to values far from the starting solution and toward that of the solid calcite (Fig. 3c). Later in Experiment 3, the effluent $^{87}Sr/^{86}Sr$ ratio increases and approaches that of the starting solution.

4. Estimation of calcite dissolution and precipitation rates

We use three, independent geochemical and isotopic measurements of effluent to estimate in-situ dissolution and precipitation rates. Our experiments are designed so that granular calcite is subjected to compression while simultaneously, fluid that is approximately saturated with calcite flows slowly through the sample. The starting composition of the fluid is constant and known, and the effluent from the compacting column is monitored for Ca, Mg, and Sr concentration, and the $^{87}Sr/^{86}Sr$ ratio of dissolved Sr. Because calcite has low solubility, small amounts of dissolution or precipitation of calcite measurably affect the fluid,

Table 2
Experiment 1 geochemistry results, JY marble substrate, < 120 μm grain size, 23 °C, 5 MPa confining pressure, 7 MPa axial stress.

Sample#	flow rate ml/min	time hr	Ca (mM)	Sr (μM)	Mg (μM)	Sr/Ca mmol/mol	Mg/Ca mmol/mol
Calcite (JY)						0.198	4.82
start fluid		0	0.592	0.111	2.18	0.188	19.6
1	0.1	0.4	0.651	1.175	31.81	1.805	27.1
2	0.01	3.3	0.619	0.345	10.39	0.557	30.1
3	0.01	8.3	0.562	0.326	10.18	0.580	31.2
4	0.01	13.3	0.540	0.260	7.47	0.481	28.7
5	0.01	18.3	0.523	0.224	6.69	0.428	29.9
6	0.01	23.3	0.548	0.208	6.42	0.380	30.9
7	0.01	28.3	0.541	0.194	7.12	0.359	36.7
8	0.01	33.3	0.543	0.187	7.12	0.344	38.1
9	0.01	38.3	0.568	0.185	5.76	0.326	31.1
10	0.01	48.3	0.594	0.192	5.72	0.323	29.8
11	0.01	53.3	0.605	0.179	5.35	0.296	29.9
12	0.01	58.3	0.623	0.185	5.35	0.297	28.9

producing a difference in Mg/Ca, Sr/Ca and $^{87}Sr/^{86}Sr$ in the column effluent relative to the starting solution. For example, when calcite dissolves it releases Sr and Ca into the fluid in proportion to the Sr/Ca ratio of the dissolving calcite. When secondary calcite forms by precipitation from the solution, it forms with a *different* Sr/Ca ratio that is determined by the Sr/Ca partition coefficient (D_{Sr}) and the Sr/Ca ratio of the solution.

The measured geochemical changes can be modeled to yield an estimate of the mean rates of dissolution and precipitation within the column in units of fraction dissolved/precipitated per unit time (or time^{-1}). With the fluid starting and presumably remaining near equilibrium, the expectation is that the only significant dissolution is driven by pressure solution at grain contact surfaces. The transit time of the fluid through the column is typically 1.02 h, which is much shorter than the 60 to 300 + hour duration of the experiments. Hence the effluent trace and isotope chemistry provides a near-real time estimate of the "reaction rate," which can then be compared directly to the measured compaction rate, which also has units of time^{-1}. The Sr isotope ratio is another measure of fluid–solid chemical interaction, but unlike the Sr/Ca and Mg/Ca ratios, it is only sensitive to calcite dissolution. During passage of the fluid through the column, the fluid $^{87}Sr/^{86}Sr$ ratio shifts gradually from the value in the starting fluid toward the value of the solid calcite, with the rate of change proportional to the calcite dissolution rate. The slower the rate of dissolution, the less the fluid $^{87}Sr/^{86}Sr$ changes during passage through the column. Changes in the fluid Sr/Ca and Mg/Ca are produced mainly in the calcite precipitation process while changes in fluid $^{87}Sr/^{86}Sr$ are produced only by calcite dissolution.

Our conceptual model is that calcite dissolution occurs on the contact surfaces between grains where contact area is low and effective stress is high. Because the total strain is small, the area of these contact surfaces is expected to be a small fraction of the total surface area of the grains. Precipitation should occur along unstressed grain surfaces in the larger pore spaces between grains provided it is not advected out of the system. The geochemical measurements allow us to independently assess the total amount of dissolution and precipitation occurring in the column, so we have also a measure of the degree to which the two are balanced during the experiments. Details of the mathematical model are presented in Supplementary Materials, Part 2.

5. Relationship between strain rate and calcite reaction rates

5.1. Direct comparison of strain and reaction rates

To begin our discussion of the relationship between reaction rate and strain rate, it is instructive to compare the two measured rates directly. The calculated volumetric strain rates and calcite reaction rates for the two experiments are summarized in Fig. 4. The strain rates measured for Experiment 3 are a little less than half those for Experiment 1. The calcite reaction rates in both experiments, assuming dissolution and precipitation rates are equal (i.e. $R_d = R_p$; Supplementary Material Part 2), are systematic, with values about 5 to 10 times smaller than the strain rates, and decreasing through time in a manner analogous to but not exactly in proportion to strain rate. Experiment 1 shows a rapid initial decrease in reaction rate. The high starting value is inferred to reflect initial rapid dissolution of fines, an inference supported by the Ca concentration analysis described below. The recrystallization rates inferred from Mg/Ca are higher than those from Sr/Ca by a factor of

Table 3
Experiment 3 geochemistry results, Water treatment marble substrate, 90–212 μm grain size, 23 °C, 10 MPa confining pressure, 15 MPa axial stress.

sample #	**flow rate ml/min**	**t h**	**Ca mmol/kg**	**Sr umol/kg**	**Mg umol/kg**	**Sr/Ca** mmol/mol	**Mg/Ca** mmol/mol	**$^{87}Sr/^{86}Sr$ (±0.001 %)**
calcite (WT)						1.283	22.17	0.708468
start fluid		0	0.591	0.85	2.0	1.44	3.38	0.710134
1	fast flush	0	0.634	2.14	21.7	3.37	34.16	0.709006
2	0.01	5	0.544	4.19	51.0	7.69	93.77	0.708719
3	0.01	15	0.590	2.84	29.8	4.82	50.51	0.708906
4	0.01	25	0.623	1.66	12.5	2.65	19.99	0.709296
5	0.01	35	0.616	1.23	7.0	2.00	11.38	0.709583
6	0.01	45	0.623	1.11	5.0	1.78	7.96	0.709756
7	0.01	55	0.646	1.09	4.0	1.68	6.24	0.709850
8	0.01	65	0.642	1.03	3.4	1.60	5.36	
9	0.01	75	0.633	1.01	3.1	1.59	4.95	0.709968
10	0.01	85	0.628	0.97	2.9	1.54	4.61	
11	0.01	95	0.626	0.97	2.9	1.55	4.58	0.709988
12	0.01	105	0.631	0.96	2.8	1.52	4.44	
13	0.01	115	0.623	0.95	2.8	1.53	4.49	0.710015
15	0.01	135	0.618	0.93	2.7	1.50	4.34	0.710018
17	0.01	153	0.626	0.96	2.8	1.53	4.54	
19	0.01	173	0.629	0.94	2.6	1.49	4.21	
22	0.01	203	0.616	0.92	2.7	1.50	4.31	0.710034
27	0.01	253	0.638	0.95	2.9	1.49	4.58	0.710066
56	0.01	543	0.606	0.89	2.5	1.46	4.16	0.710116
74	0.01	723	0.611	0.90	3.9	1.48	6.39	0.710084
B1		~25	0.578	0.82	2.5	1.43	4.34	
B4		~320	0.589	0.85	2.2	1.45	3.71	
start fluid (2)		0	0.588	0.85	2.2	1.44	3.73	

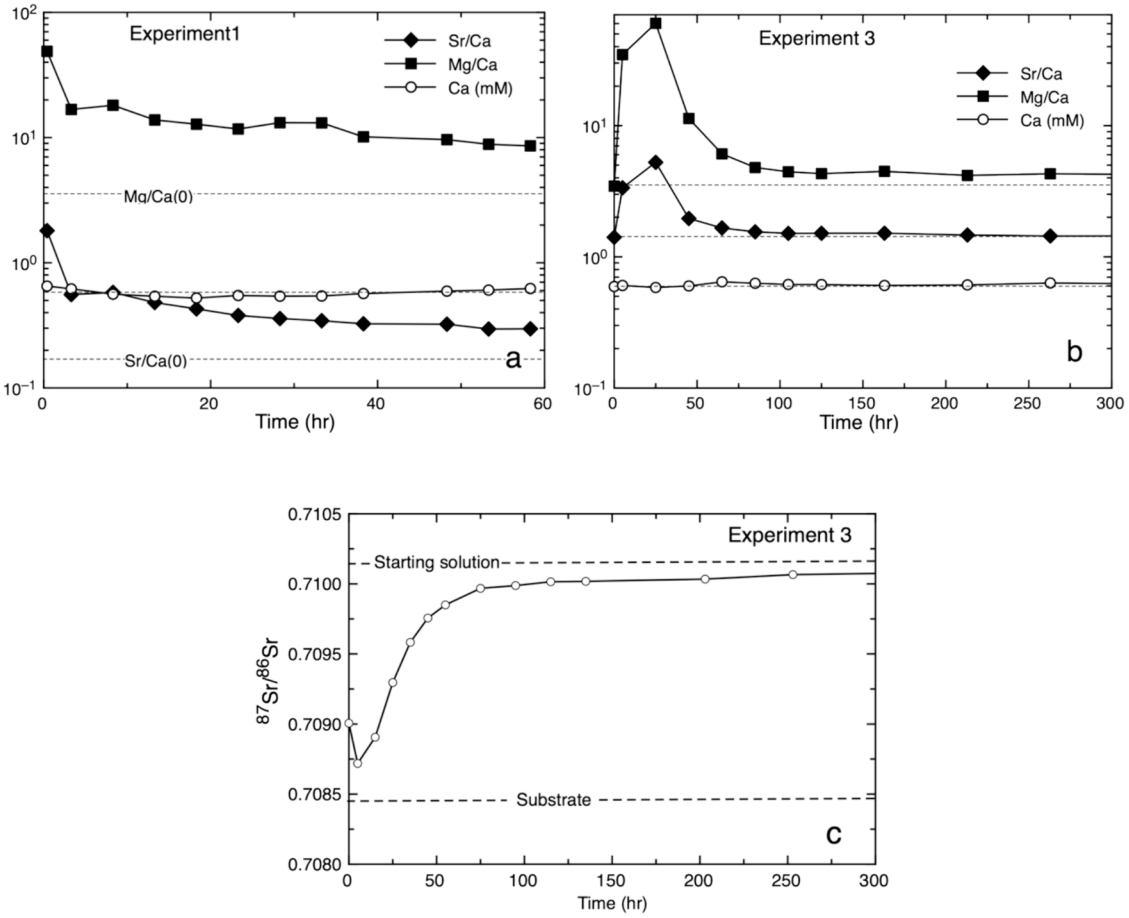

Fig. 3. Chemical data (a) for Experiment 1 and chemical (b) for Experiment 3 and Sr isotopic data (c) for Experiment 3. In Experiment 1 the Sr/Ca and Mg/Ca data are used to calculate the calcite reaction rates. In Experiment 3, the starting fluid Sr/Ca and Mg/Ca were set to be close to the equilibrium values so they are somewhat less sensitive for determining reaction rates, but their relative constancy in the experiment makes the interpretation of the Sr isotope data simpler. Calcium concentration is set to be near the equilibrium value and stays nearly constant during the experiments.

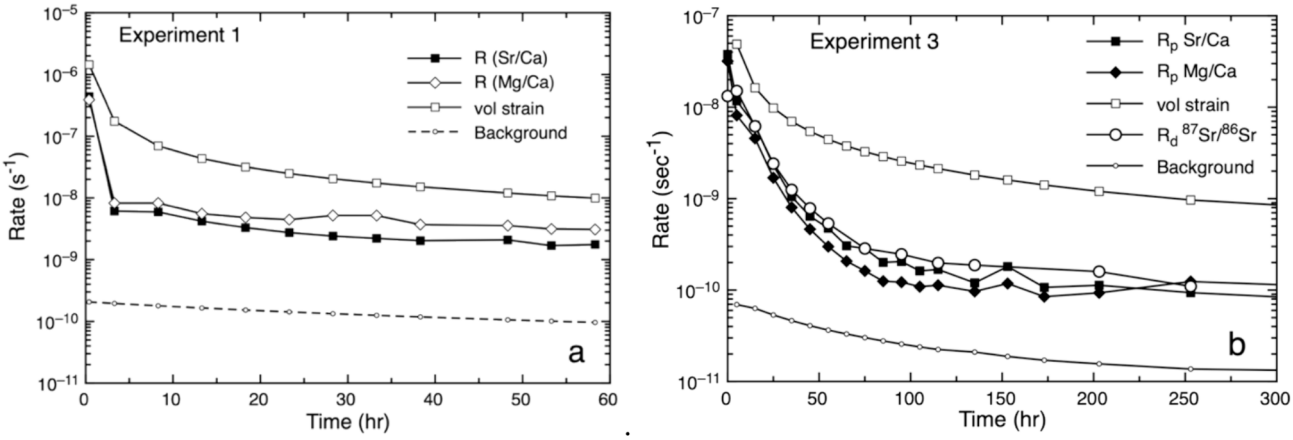

Fig. 4. (a) Calcite-fluid recrystallization rates (R, in units s^{-1}) calculated from fluid Sr/Ca and Mg/Ca versus time in benchtop Experiment 1 with applied stress of 2 MPa. D values of 0.05 for Sr/Ca and 0.01 for Mg/Ca were used, but the results are insensitive to these assumed values within their likely range. (b) Reaction and strain rates for Experiment 3 with applied stress of 5 MPa; dissolution rate, R_d, based on $^{87}Sr/^{86}Sr$ measurements, and precipitation rate, R_p, based on Sr/Ca and Mg/Ca. Approximate volumetric strain rates are from the logarithmic fit to the data (Fig. 3b). Background exchange rates are based on the experiments of Chanda et al. (2019) using the geometric surface areas for our grain packs (3 m^2/mol for Experiment 1 and 1 m^2/mol for Experiment 3).

about 1.5 in Experiment 1, but lower by factors of 1.2 to 1.5 in Experiment 3. These differences cannot be changed by adjusting the partition coefficients within reasonable bounds, and indicate that Mg/Ca partitioning may be more sensitive to mineral and fluid compositional variations than is Sr/Ca partitioning (Mucci and Morse, 1983). To simplify discussion, in the following we focus mainly on the rates determined from Sr/Ca and $^{87}Sr/^{86}Sr$.

The ratio of reaction rate to strain rate in Experiment 1 increases

from 0.04 to 0.2 during the course of the experiment (Fig. 6a). The Ca concentration analysis suggests that $R_d = R_p$ within 10 to 20 %, so the derived rates from the simple analysis are relatively accurate (Supplementary Material, Part 3). In Experiment 3, there is an extended early pulse of high reaction rate, even though fines were absent from the calcite. The reaction rate-to-strain rate ratio based on Sr/Ca and $^{87}Sr/^{86}Sr$ and using the logarithmic fit to the strain data shown in Fig. 3b, is about 0.3 at 25 h, decreases systematically to 0.08 to 0.1 at 80 h and then gradually increases toward 0.15 at 200 to 300 h. The latter part of this sequence is similar to that of Experiment 1. Initial differences and later convergence suggest that mechanisms other than pressure solution, such as fine dissolution and cracking, may be controlling the fluid chemistry early in experiments. The dissolution rates derived from $^{87}Sr/^{86}Sr$ in Experiment 3 are slightly higher than the recrystallization rates derived from the elemental ratios. The small difference implies that $R_d > R_p$, meaning there is a small amount of net dissolution.

5.2. The geometric relationship between dissolution and strain

Our data provide a measure of the total rate of calcite dissolution and precipitation occurring in the column, but the strain due to pressure solution is determined by the dissolution *per unit area on the grain contact surfaces* (e.g. Zhang and Spiers, 2005a). In the following section, we describe how calculated recrystallization rates relate to pressure solution strain rates, and how they compare to the measured strain rates in the experiments. We use the standard model for pressure solution strain first proposed by Weyl (1959) and more recently parameterized by Zhang et al (2010). This model is illustrated in its simplest form in Fig. 6, adapted from He et al (2013). Although the model is a simplification of the actual sample geometry, it is useful in that it provides relationships between strain, grain size, reaction rates, and diffusion effects that can be used to assess general features of compaction experiments (Zhang and Spiers, 2005a; Zhang et al., 2010).

In our discussion we focus on dissolution at the grain contact surfaces because it is responsible for the observed sample volume reduction. Our discussion of reaction rates is also focused on dissolution and the geometric controls on pressure solution rates on grain contacts. As noted in Zhang et al (2010) and elsewhere, dissolution rates can be affected by precipitation rates in the larger pores if that process is sluggish enough to affect the saturation state of the fluid phase on grain boundaries. Our geochemical approach constrains both dissolution and precipitation rates, which we can show to be subequal, although there is evidence for slightly faster dissolution. The rate equations for both processes are essentially indistinguishable at small strains (Zhang et al. 2010) so our conclusions based on dissolution rates would not be affected if precipitation control is also important. It should also be noted that excess dissolution of 10^{-10} s^{-1} over the course of 200 h (Figure S10) would result in removal of only 0.007 % of the solid mass and hence does not contribute significantly to measured strain.

Fig. 6 represents two spherical grains of diameter *d* with a circular contact surface of radius *a*, the area of the contact surface is πa^2, the approximate surface area of an individual grain is πd^2, and the grain volume is $\pi d^3/6$. If dissolution on the contact surfaces is causing each surface to migrate toward the grain center at a velocity v_s, which is the area-normalized dissolution rate in m/s, the distance between the two grain centers decreases at a rate $2v_s$. The distance between the two grain centers can be called 2x where, at small strains, $x \approx (d^2/4 - a^2)^{0.5}$. The strain inherent in this model system, relative to two spheres that are barely touching, is $\varepsilon = 1 - 2x/d$. The instantaneous strain rate is $d\varepsilon/dt = v_s/x$. For small strains of order 1 %, $x \approx d/2$, and strain rate can be approximated as $d\varepsilon/dt \approx 2v_s/d$. The fractional rate of dissolution of the grains, which is the reaction rate as measured geochemically in our experiments, is: $R_d = 12v_s a^2/d^3$ $(=2v_s\pi a^2/(\pi d^3/6) = 2v_s A_{contact}/V_{grain})$ The ratio of this reaction rate to the volumetric strain rate (data in Fig. 5), for the spherical grain model is:

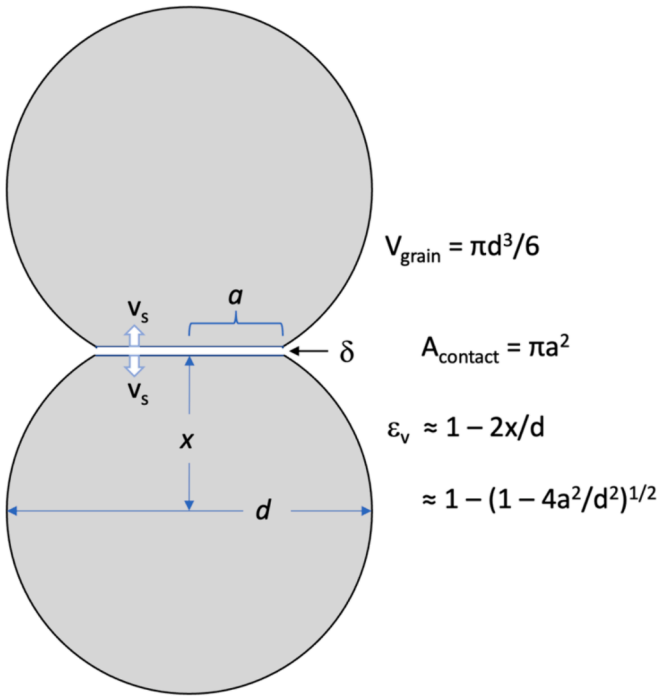

Fig. 6. Illustration of the relationships between grain contact surface area, strain due to dissolution on the contact surface, grain diameter, and grain volume, adapted from He et al. (2013). The velocity v_s is the dissolution rate averaged over the contact surfaces. The width or aperture of the contact zone is δ, which affects diffusion of dissolution products to the intergranular pore space. This 2-grain model is sufficient to describe any packing geometry of uniform spherical grains.

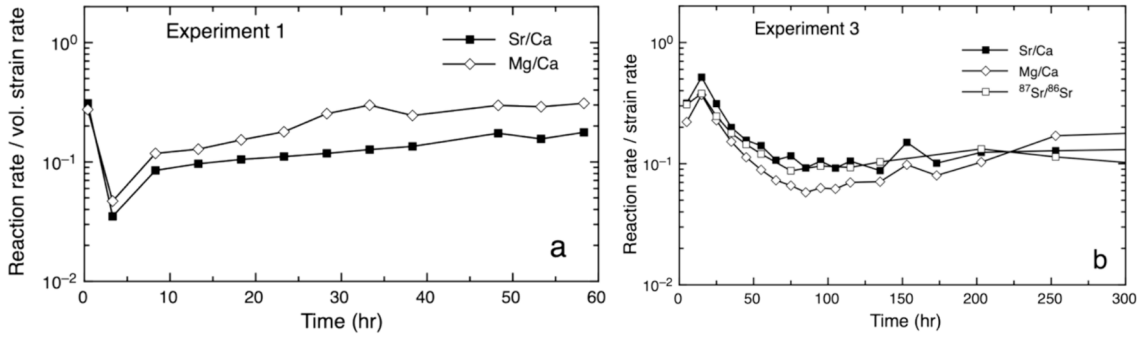

Fig. 5. Reaction rate – strain rate ratios for (a) Experiment 1 and (b) Experiment 3. The results from Mg/Ca are slightly higher for Experiment 1 and lower for Experiment 3.

$$R_d = 6\frac{A_{cont}}{A_{gr}}\frac{d\varepsilon_v}{dt} = \frac{6a^2}{d^2}\frac{d\varepsilon_v}{dt} \quad (1)$$

Equation (1) applies if all strain is due to pressure solution on grain contact surfaces, but the measured reaction rate (R_d) does not distinguish between reaction and diffusion control. The result is that the reaction rate as we measure it relates to the pressure-solution strain rate, but only though the ratio of contact surface area to total grain surface area.

Equation (1) indicates that the ratio of reaction rate to strain rate is a measure of the grain contact surface area, and through the relationships depicted in Fig. 6, also a measure of strain. We can first ask whether the implied a/d values based on the measured values of ($d\varepsilon_v$/dt)/R are reasonable given the amount of measured strain in the experiments. In Fig. 7, we show the inferred a/d values, calculated using Equation (1) and the data in Fig. 5, and how they change with time in the two experiments, as well as the "total strain" calculated from the inferred a/d and $\varepsilon = 1 - 2x/d$.

In Experiment 1, using the Sr/Ca data, the behavior is qualitatively as expected. As the grain pack compacts during the experiment, a/d increases, meaning the area of the contact surfaces increases. The total amount of strain inferred from the a/d values based on Sr/Ca is in the range 2 to 4.5 %, which is in the right range, but the inferred increase in strain between 10 h and 60 h (4 %) is much larger than measured (0.4 %). For Experiment 3, the first 60 to 80 h of the experiment are much different from what is expected when we use the logarithmic fit (Fig. 3b) to describe the strain rate versus time. Between the start and about 50 h, the inferred values of a/d are much higher than expected, reflecting high reaction rates, peak at about 15 h and then decrease until about 80 h. This behavior is an indication that the initial deformation of the sample was more complex than can be approximated by pure pressure solution. Starting at 80 h, the geochemically inferred strain systematically increases from about 2 to 3 % to about 5 %. As with Experiment 1, the total amount of strain is reasonable, but the increase in strain between 80 and 250 h is larger than the *measured* strain increase, which is less than 0.1 % (Fig. 3b). The conclusion from this analysis is that the reaction rates measured in Experiment 1 with Sr/Ca are close to what is needed to explain the strain by pressure solution, and in Experiment 3 the reaction rates are initially too high relative to strain rates, indicating that there was additional reaction that was not contributing to strain. Early in experiments, the contact stresses are the highest, which may result in fracturing, leading to changes in surface area and angularity of grains and causing enhanced dissolution (e.g. Heidug 1991).

5.3. Comparison of measured reaction rates and strain rates

The next stage of our analysis is to evaluate the area-normalized pressure-induced dissolution rates that are implied by our strain rate data, by converting them to units normally used for reaction rates (mol/m^2/s) and comparing them to the measured reaction rates. The dissolution rates needed to account for the strain by dissolution on grain contacts can be calculated from the strain rate and the grain size. Using the expression derived above, the dissolution velocity is $v_s = (d\varepsilon/dt)(d/2)$. The velocity in m/s can be converted to mol/m^2/sec by multiplying v_s by the density of calcite in mol/m^3 (2.7×10^4). The resulting rates (Fig. 8), 3.5×10^{-7} to 2×10^{-9} mol/m^2/s, are about 85 % to 0.5 % of the calcite dissolution rate constant at 25 °C used by Zhang et al (2010) (4×10^{-7} mol/m^2/s).

The measured reaction rates are related to the rates calculated from

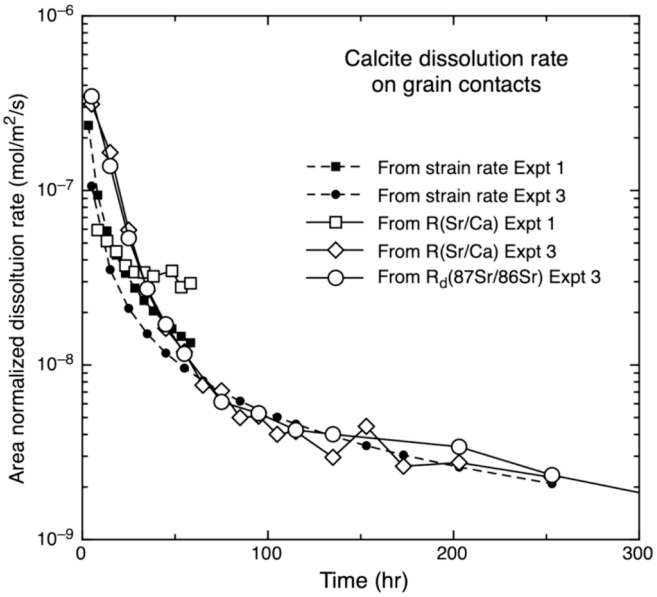

Fig. 8. Dissolution rates of calcite on grain surfaces calculated from measured strain rate and from the measured reaction rates divided by $6a^2/d^2$. The value of $6a^2/d^2$ used is the Zhang et al. (2010) model value based on measured strain (Fig. 7). For comparison, the rate constant for calcite dissolution is about 4×10^{-7} mol/m^2/s at 25 °C (Zhang et al., 2010). Grain size used for this calculation is 80 μm for Experiment 1 and 160 μm for Experiment 3.

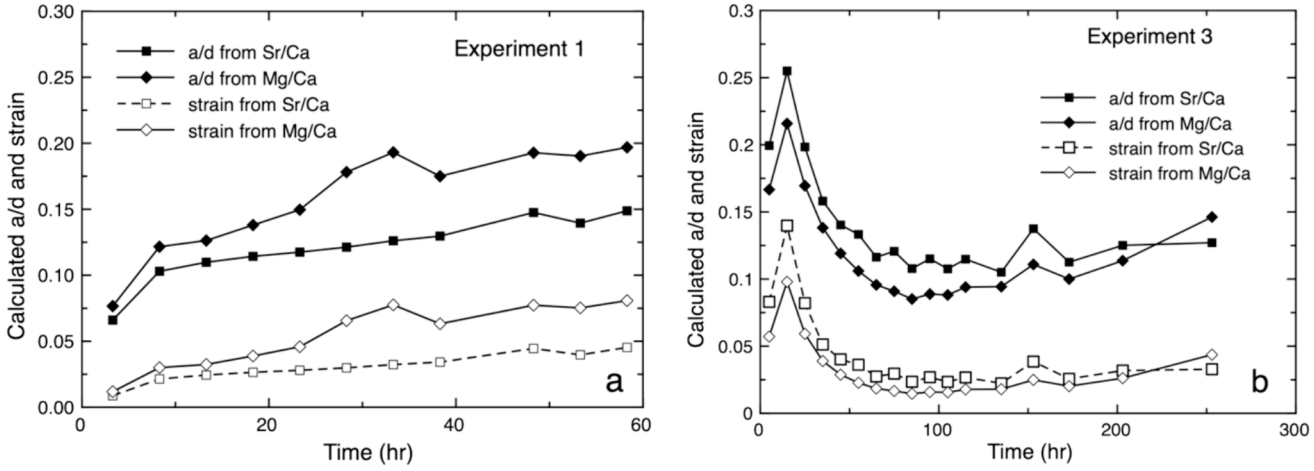

Fig. 7. Values of a/d and strain calculated from Sr/Ca and Mg/Ca using Equation (1) and the measured ratio of calcite dissolution/precipitation rate and strain rate as depicted in Fig. 5. Also shown are the strain values calculated from a/d values for Sr/Ca and Mg/Ca data using the geometric relationships between the dimensions *a*, *x*, and *d* from the uniform sphere model (Fig. 6). (a) Experiment 1. (b) Experiment 3.

strain rate by the factor $6a^2/d^2$. To make the comparison we use the $6a^2/d^2$ values that are "predicted" by the Zhang et al (2010) model based on total strain (Fig. 8). For Experiment 1, the measured rates are close to the rates deduced from strain rate during the first half of the experiment and then diverge to higher rates. For Experiment 3, the measured rates agree with the rates deduced from strain rate after 50 h but are too high before that. The high values suggest that there was additional reaction that was not contributing to strain, possibly due to fracturing, reducing grain size and exposing new highly reactive grain surfaces. An important observation is that measured reaction rates are close to what is needed to account for the measured strain and strain rates after roughly 80 h.

5.4. *Microstructural observations of grain boundary structure.*

Estimates of a/d from the geochemical data, mostly in the range of 0.08–0.16 (Fig. 7) can be compared directly to microstructural measurements. The a/d parameter applies strictly only for grain boundaries that can be characterized by a single contact area and grain diameter using a close packing of spheres as a model, but it is useful as a reference in analyzing the more complex situation involving angular grains of a range of sizes. The evolution of grain boundary structure determines the relative contribution of subcritical cracking and pressure solution as well as whether pressure solution is reaction or diffusion limited, by way of determining the stress intensification factor and the size of the contact surfaces. We can gain insight by examining SEM images of experimental material prior to and after reaction (Fig. 9).

The contacts between grains are not uniform; they vary from ~ 1 μm to ~ 30 μm in width. Using an average grain diameter of 160 μm, this puts a/d between 0.01 and 0.2, roughly in agreement with the estimate from the measured strain to reaction rate ratios (Fig. 8). The variation is large, which is not surprising given the microstructure of the grain pack. The average value of a/d is close to 0.10 or 0.15, which is the range inferred from the experimental data after total strain had reached about 4 %.

There are several ways that the geometry of our samples contrast with a close packing of uniform spheres. Firstly, the general shape of calcite grains is more cuboid than round, thus they have points, edges and faces instead of uniform curved surfaces. The initial material is rhombs of calcite with sharp corners. As opposed to the one type of contact possible between spheres, there are six: point on point, point on edge, point on face, edge on edge, edge on face and face on face. There is evidence in the SEM images that pressure solution dominates where contacts are formed by points or edges, which would have the highest stress (Fig. 9g,h). The actual contact area of each of these is likely further complicated by roughness. Secondly, the range of grain size and shape in our experiments leads to a different porosity evolution than expected from uniform spheres. The minimum porosity of a close packing of uniform spheres is ~ 0.26. For a random packing of spheres the minimum is 0.36, while our samples vary from ~ 0.32–0.27 over the course of an experiment (see Supplementary Material). The observations from our experiments are different from the expected porosity evolution due to the uniform truncation of close-packed spheres, although as noted below, predictions using the simple geometric model with unform spheres are not far from our experimentally determined strain rates.

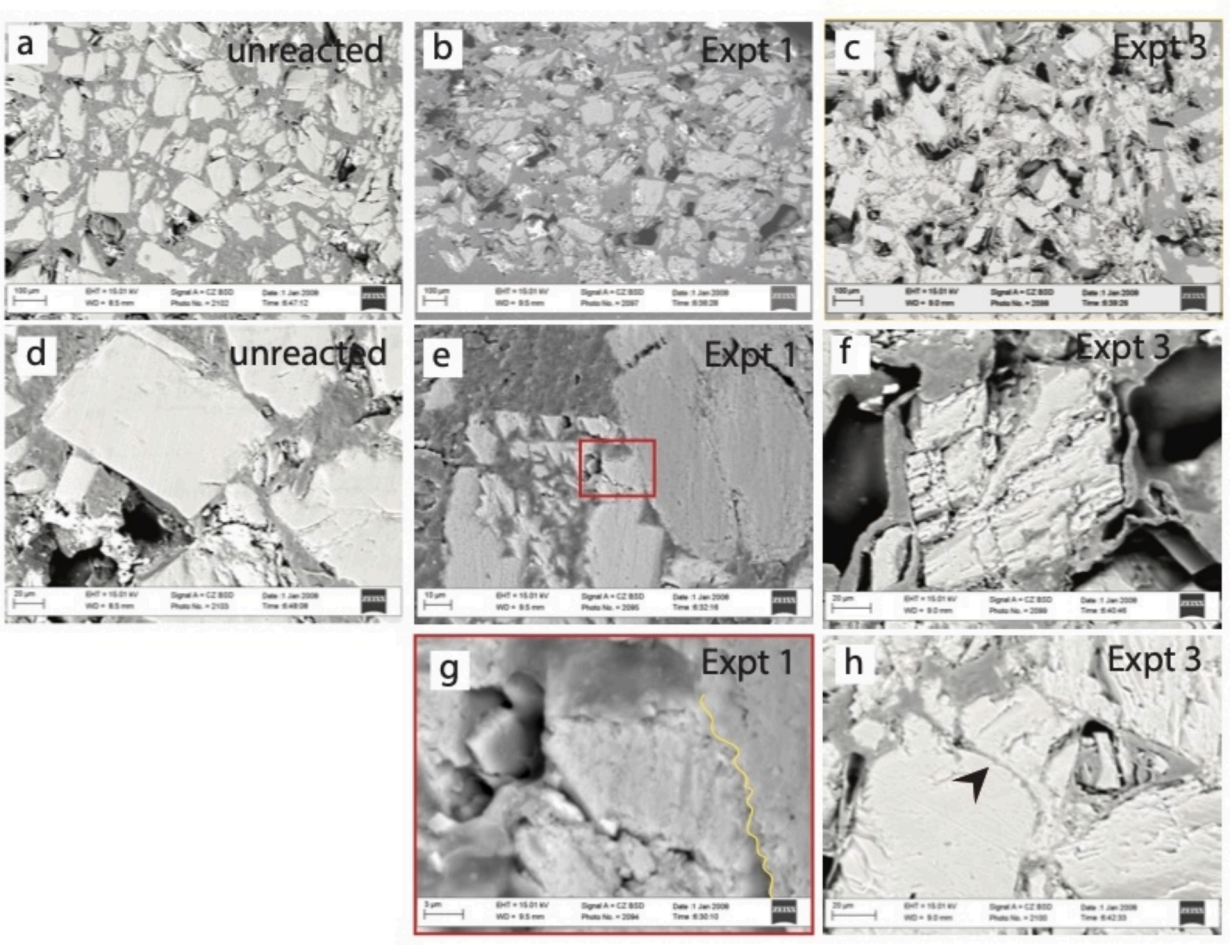

Fig. 9. SEM images of experimental material. Overviews of a) unreacted material, b) Experiment 1 at 2 MPa nominal axial stress and c) Experiment 3 at 5 MPa nominal axial stress. Grain-scale views of d) unreacted material, e) experiment 1 and f) experiment 3. g) close-up view of impinging, rough contact from Experiment 1. h) evidence of grain-indentation accompanied by fracturing from Experiment 3.

The structure of individual contacts also varies from a simple planar circular contact, and implies that the "island-channel" model of grain contacts (e.g. deMeer et al., 2005) is a better description of the grain contacts in our experiments than the depiction of Fig. 6. To quantify this, the roughness of individual calcite grains was measured using a vertical scanning interferometer (Zygo NewView 7300). Calcite grain surfaces have structures on a range of scales. On the scale of grains, steps and cleavage plains separate relatively flat surfaces with relief on the order of 10 μm (Fig. 10). Along these relatively flat surfaces, there is nanometer-scale roughness (Fig. 10e). This roughness means a contact with 100's of square microns of nominal area has only several square microns of real contact area. This suggests that additional factors may need to be added to the expression for surface reaction rate that account for the difference between actual contact area undergoing dissolution, nominal grain scale contact area, and the corresponding differences in stress. The roughness data also imply that the channels between grains have an aperture of 10's of nanometers in contrast to the 1 nm commonly assumed in diffusion models (e.g. Spiers and Schutjens, 1990), and substantial tortuosity, both of which would influence diffusion.

It is evident that fracturing processes play a role in both experiments 3. There are some fractures present in unreacted materials, which may have been induced during the grinding, sieving and initial handling; however, most of the fractures evident in reacted samples occurred during compaction. The sample from Experiment 3 exhibits the most substantial fracturing (e.g. Fig. 9f), which may help explain the excess reaction inferred by geochemical measurements (Fig. 7) and discussed in section 5.3.

6. Comparison of model predictions and experimental results

6.1. Thermodynamics of thin film vs. island channel models of pressure solution

The key concept for describing pressure solution in calcite is that the solubility of calcite increases with pressure or interfacial normal stress at constant temperature. Consequently, referring to the model diagram (Fig. 6), if a stress is applied to a grain pack, and a normal stress is concentrated on the grain-grain contact surfaces, the fluid pressure within the fluid film at those contacts is in equilibrium with that normal stress and is higher than that in the open pore space (Lehner, 1990). The resulting normal stress difference should cause the calcite to dissolve at the contact surfaces and re-precipitate in the pores. The increase of calcite solubility with hydrostatic pressure can be written approximately in the form:

$$K_{eq}(P) = K_{eq}(P_0)exp\left(\frac{P - P_0}{P_r}\right) \quad (2)$$

where K_{eq} is the solubility product constant, and P_r is a scaling pressure equal to $RT/v_{cc} \approx 67$ MPa at 25 °C (Zhang et al., 2010) and using the 1 atmosphere molar volume of calcite. Consequently, if the effective excess *fluid* pressure on the grain contacts is denoted as p_{eff}, excess solubility can be written as:

$$K_{eq}\left(P + p_{eff}\right) = K_{eq}(P)exp\left(\frac{p_{eff}}{P_r}\right) \quad (3)$$

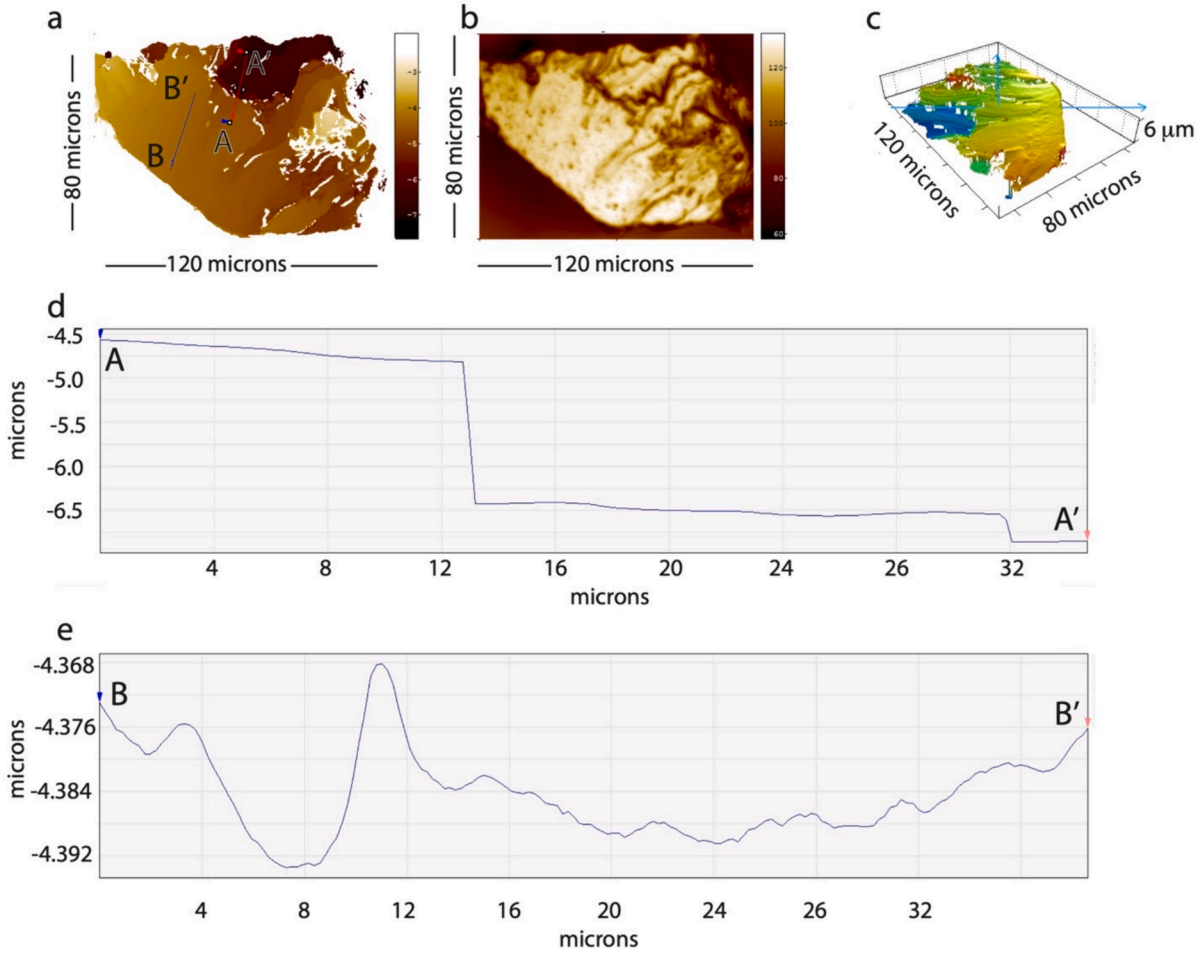

Fig. 10. Results of vertical scanning interferometry of calcite grain. a) contour map of grain surface, b) raw data showcasing fine structure, c) volume rendering of sample surface, d) line profile across large steps, e) line profile across smooth surface.

In a calcite grain pack held at a hydrostatic pressure, P, the solubility of calcite overall will be higher than at 1 bar, but the calcite will have no tendency to dissolve if the fluid has equilibrated with the calcite at pressure P. The calcite at the grain contacts would tend to dissolve only because the effective pressure *in the fluid film* within the contacts is higher by p_{eff}. In the model we assess in the next section, the effective pressure on the fluid is assumed to be: $p_{\mathrm{eff}} = \mathrm{B}\sigma_{\mathrm{e}}$, where σ_{e} is the applied stress on the grain pack and B is a geometric factor that accounts for the concentration of stress on the grain contact surfaces (Zhang et al., 2010).

Another model for the grain contacts, sometimes referred to as the "island-channel" model, is that they are rough, and stress is concentrated at asperities. In this case, all or most of the calcite dissolution could occur at the asperities where stresses may reach GPa levels, at least until the asperities are dissolved away. In this model the pressure in the grain contact fluid is equal to that in the pores and the increase in calcite solubility is due to stress effects on the thermodynamic stability of the solid at the asperities. If the length scale of the islands or asperities within the grain-grain contact regions is much smaller than the contact radius (a in Fig. 7), then Lehner (1990, 1995) has shown that equation (3) still applies, in an approximate sense, at the grain-grain contact scale. If the islands are larger, however, the solubility would be a function of the normal and shear stresses on the solid asperities, but a highly simplified version would just account for the concentration of normal stress, and could be written as:

$$K_{eq}(\sigma_{gb}) = K_{eq}(P_0)exp\left(\frac{(\sigma_{gb}/A_{asp})^2/K_{cc}}{P_r}\right) \quad (4)$$

where K_{cc} is the bulk modulus of calcite (about 70 GPa), σ_{gb} is the average stress on the grain boundaries (=Bσ_{e}), and A_{asp} is the fractional area of the asperities on grain contact surfaces. The expressions in equations (3) and (4) are equal when $A_{asp} = (p_{eff}/K_{cc})^{1/2}$, which occurs for plausible values of A_{asp} in the range 0.02 to 0.1 (assuming that $\sigma_{\mathrm{gb}} = p_{\mathrm{eff}}$) which also are consistent with our observations of grain contacts discussed in Section 5.

It is worth noting that the formulation for the pressure-dependence of calcite solubility has some uncertainty, especially for pressures greater then 100 MPa. For example, McDonald and North (1974) measured the increase of calcite solubility with pressure and found that the scaling pressure was 43.5 MPa, equivalent to $\Delta V_{\mathrm{r}} \approx 5.7 \times 10^{-5}$ m^3/mol, which is about 50 % larger than the molar volume of calcite. The calcite log K_{eq} data from the Soltherm thermodynamic database (Palandri, 2015), which has solubility parameterized to 500 MPa, can be fit better with $P_r \approx 90$ MPa, but a good fit requires a polynomial rather than the exponential form. For our purposes we use the formulation of Equation (3) with $P_r = 67$ MPa, since use of the other values would not change our conclusions significantly.

6.2. Pressure solution flow laws

One model for pressure solution is that the rate of dissolution of calcite at the grain contacts is controlled by diffusion of calcite dissolution products through a thin film to the open pores. As discussed above, the same concept applies to grain contacts with a very fine island and channel structure (Lehner 1990,1995). The rate of this diffusive flux is proportional to calcite solubility (with suitable caveats because it can be affected by the species in solution), so it is expected that the compaction rate ($d\varepsilon/dt$) will vary with the effective pressure on the grain boundary fluid as:

$$\frac{d\varepsilon}{dt} \propto exp\left(\frac{p_{eff}}{P_r}\right) - 1 \quad (5)$$

The diffusion-limited compaction rate also depends on the radius of the grain contact surfaces and the effective thickness and viscosity of the fluid film (Zhang et al., 2010).

A key point for estimating surface reaction-controlled dissolution rates is the effect of increasing solubility with pressure on dissolution rate. In general, calcite dissolution rate (R_s) is written in the form:

$$R_s = k_s A\left(1 - Q_{sp}/K_{eq}\right)^n \quad (6)$$

where n is reaction order, determined empirically and typically in the range 1 to 4 (e.g. Adkins et al., 2021) and A is a number between zero and 1 that can account for the density of reactive sites per unit total surface area of solid. Hence, using the pressure dependence of K_{eq} from Equation (3), the effect of the excess grain boundary stress on dissolution rate would be of the form:

$$R_s = k_s A\left[1 - exp\left(\frac{-p_{eff}}{P_r}\right)\right]^n \quad (7)$$

And hence:

$$\frac{d\varepsilon}{dt} \propto A\left[1 - exp\left(\frac{-p_{eff}}{P_r}\right)\right]^n \quad (8)$$

The solubility of calcite as a function of pressure (Equation (3) is relatively straightforward to estimate because it is controlled by thermodynamics. Surface reaction rate (Equation (6) is different because it is influenced by other factors. An important aspect of Equations (7) and (8) is that dissolution rate and strain rate reach a limiting value as stress increases so that at high effective stress, there is little dependence of strain rate on stress unless stress affects A.

Accounting for the geometric factors implied by Fig. 6, the expression for diffusion-limited compaction rate ($d\varepsilon_{\mathrm{d}}/dt$) is (ZSP, 2010):

$$\dot{\varepsilon}_d = \frac{DSC}{d^3}\left(exp\frac{p_{eff}}{P_r} - 1\right)f_d \quad (9)$$

The parameter product DSC includes the ionic diffusivity ($D=10^{-10}$ m^2/s at 25 °C), the film thickness on the grain contact surfaces ($S \approx 10^{-9}$ m), and the solubility of calcite at 0.1 MPa and 25 °C in units of volume/volume ($C \approx 2.13 \times 10^{-6}$). For the surface reaction-controlled (dissolution-limited) compaction rate (ε_s) the expression is (adapted from ZSP, 2010):

$$\dot{\varepsilon}_s = \frac{k_s A}{d}\left(1 - exp\frac{-p_{eff}}{P_r}\right)^n f_s \quad (10)$$

Equation (10) is different from that in ZSP (2010) but gives the same results for $\sigma_{\mathrm{eff}} < 10$ MPa, n = 1 and A=1. The geometrical factors f_d and f_s are, for small strains $f_s \approx 6$ and $f_d \approx 24d^2/a^2$. Equation (10) shows that the *maximum strain rate* occurs when $p_{\mathrm{eff}}/P_{\mathrm{r}} \gg 1$. Dong et al (2018) reported calcite dissolution rates in seawater up to 25 MPa and showed that k_s increases by about 3x above 7 MPa, a factor we have not included in our modeling. Variations in the mechanism of dissolution (e.g. Adkins et al., 2021) can change the value of n, and passivation by fluid components such as Mg^{2+}, Mn^{2+}, SO_4^{2-} (Zhang and Spiers, 2005a) would affect A.

Equations (5) to (10) apply if dissolution is controlled by the chemistry and thermodynamics of the fluid in the intergranular film and does not include the effect of stress on the thermodynamic stability of the solid phase at the contact surfaces (DeBoer, 1977; his equation (7). The alternative model is that the fluid pressure at the grain contacts is *equal to* the pressure in the pore fluid and the dissolution on the grain contact surfaces is concentrated at asperities and caused by the increase in free energy of the solid phase in response to stress. The formulation of that model, discussed further below, parallels equations (6) to (10) when the island-channel structure is very fine (Lehner 1990, 1995), but for a coarse asperity, the exponential term would be replaced by that in equation (4).

6.3. Subcritical cracking creep flow law

For completeness we also estimate what is predicted from the theory of compaction controlled by subcritical cracking creep (SCC). Estimates of strain rates from SCC can be made using the empirical flow law of Brantut et al. (2013). Rates obtained from this flow law require the use of parameters that are acquired experimentally, but the estimates have been shown to be insensitive to small differences in parameter values within reasonable ranges (Brantut et al., 2014):

$$\dot{\varepsilon}_{SCC} = \dot{\varepsilon}_0 exp\left(\frac{Q - Q_{peak}}{\sigma^*}\right) \tag{11}$$

where $\dot{\varepsilon}_{SCC}$ is the strain rate due to SCC, $\dot{\varepsilon}_0$ is the reference strain rate at which other parameters are derived (for our purposes $\approx 10^{-6}$ s^{-1}), Q is the effective axial stress, Q_{peak} is the peak stress at the reference strain rate, and σ^* is the activation stress. For our experiments, the exponential term is of order 0.01, so the predicted SCC rates are order 10^{-8} s^{-1}, which is not far from the observed strain rates. The parameters used for our calculations are listed in Table 1 and the results for both Experiment 1 and Experiment 3 plotted in Figs. 12 and 13.

6.4. Thin film model

In our experiments, we measured strain and strain rate and have a reasonable estimate of average grain size, so it is possible to predict strain rate versus time using equations (9) and (10). (see Table 4).

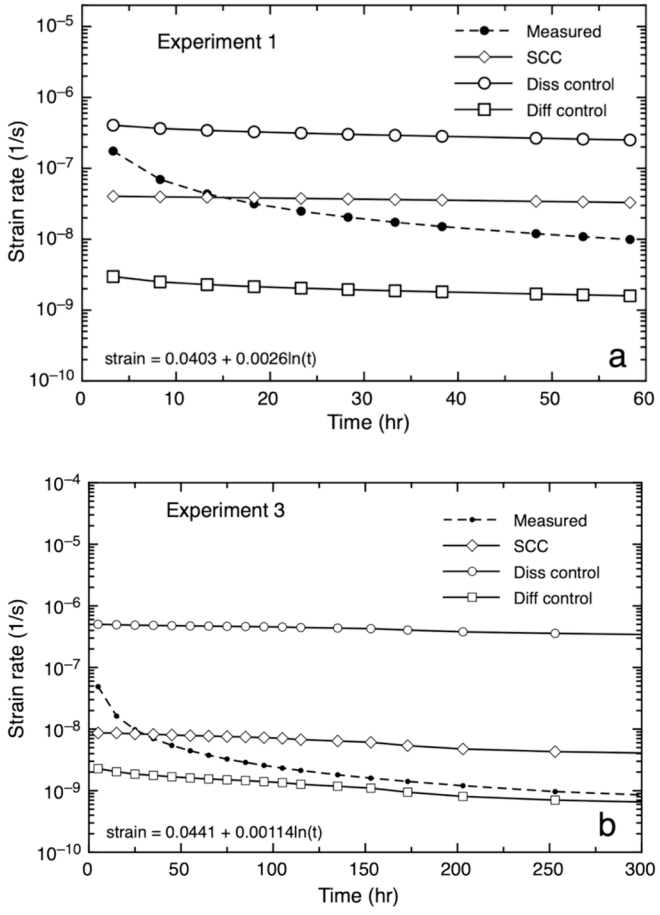

Fig. 11. Calculated and measured strain rates using the ZSP (2010) model with specified strain, n = 3 for reaction rate kinetics (equation (10) and DS=10^{-19} m^3/s for the diffusion-control model (equation (9). (a) Experiment 1 and (b) Experiment 3. SCC curves are predictions of the Brantut et al. (2014) model for subcritical crack-controlled creep.

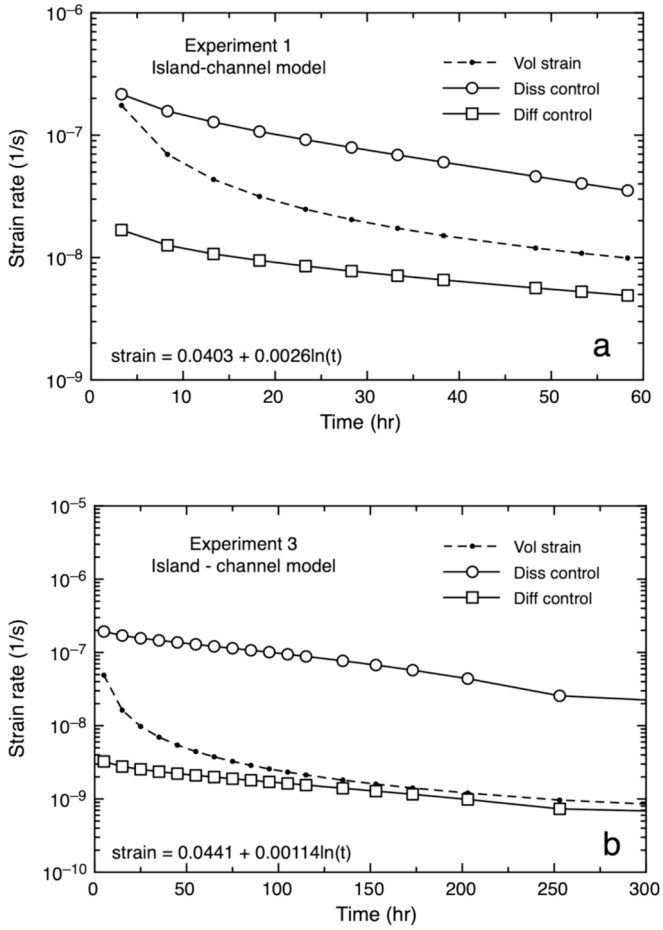

Fig. 12. Calculated and measured strain rates using the proposed island-channel version of the ZSP (2010) model with specified strain, n = 3 for reaction rate kinetics, K_{cc} = 70 GPa, and DS=10^{-18} m^3/s for the diffusion-control model (equations (9) and (10), but using the exponential expression from equation (4). (a) Experiment 1, using A_{asp} = 0.04 and (b) Experiment 3 using A_{asp} = 0.08.

The results are shown in Fig. 11 and include the SCC model. A summary of the parameters used in the models is provided in the Supplementary Materials, Part 4.

For both experiments we use n = 3 (equation (10) for calcite dissolution kinetics, based partly on the results of Dong et al (2018) who showed that pressure had little effect on reaction order, and other studies showing reaction order between 2 and 4.5 (cf Adkins et al., 2021). Using n = 2 would not change the results significantly. We use the equation for log K_{sp} given in ZSP (2010), and the values they use for k_s (1.6×10^{-11} m/s) and DS (10^{-19} m^3/s). For Experiment 1 the SCC model gives the right order of magnitude for the strain rate but does not provide a good fit to the measurements. The diffusion-control model rates are too low, and the dissolution control model rates are too high and neither captures the time dependence of the rates. For Experiment 3, where the applied stress is higher, the SCC model again gives the right order of magnitude rates, but only the diffusion-control model provides a good fit to the data, and only for the second half of the experiment. The dissolution-control model rates are too high overall and do not change enough with time but can account for the high strain rates early in the experiment. If absolute strain is decreased, the diffusion-control model can be made to fit the measurements for Experiment 1, but for Experiment 3 both pressure solution model rates increase by large factors and make the agreement with measurements worse. Although there is uncertainty due to the model rate dependence on total strain, it appears from application of the models that the strain rates we measured may

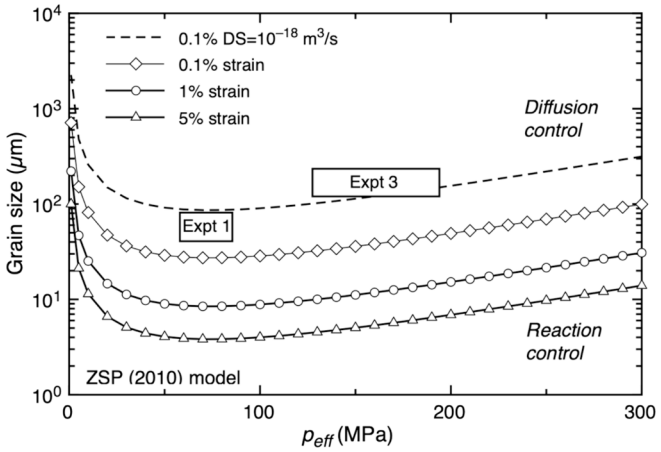

Fig. 13. Calculated process predominance diagram for diffusion- and reaction-control of pressure solution creep in calcite grain packs based on equations (9) and (10) (n = 3, P_r = 67 MPa, DS=10^{-19} m^3/s, $k_s = 1.6 \times 10^{-11}$ m/s). Dashed curve shows the effect of increasing DS to 10^{-18} m^3/s. Average grain size and (calculated) effective stress range for Experiments 1 and 3 also shown. Slower reaction rates would move all curves to larger grain sizes. For the dissolution kinetic formulation given in ZSP (2010) the critical grain size is 3 μm at 0.1 % strain decreasing to 0.5 μm at 5 % strain, with no dependence on grain boundary stress.

Table 4
Parameters used in calculations using the Brantut et al (2013) flow law.

Parameter	Value
Grain size, d	100 μm
Molar volume of calcite,Ω	3.69×10^{-5} $m^2 mol^{-1}$
Gas constant, R	8.3145 J mol^{-1} K^{-1}
Temperature, T	297 K
Reference strain rate, $\dot{\varepsilon}_0$ [a]	10^{-6} s^{-1}
Activation stress, σ^* [b]	2 MPa
Peak stress, Q_{peak} [a]	10.4 MPa for Experiment 1; 14.5 MPa for Experiment 3

[a] extrapolated from Wang et al. [2018].
[b] from Brantut et al. [2014].

have a significant component of reaction control, and either there is a transition from reaction toward diffusion control or the reaction rates vary with time more than the model predicts.

6.5. Island-channel model

The model results shown in Fig. 11 can be compared to analogous models using equation (4) to describe the effect of stress concentration on grain contacts on the solubility of calcite. This type of model introduces another parameter (A_{asp}) and would be more consistent with a greater film thickness S (deMeer et al., 2005). For illustration, the model results (Fig. 12) are calculated for DS=10^{-18} m^3/s and constant A_{asp} = 0.04 for Experiment 1 and 0.08 for Experiment 3. The values of A_{asp} are chosen to bring the model rates close to the measured rates but are consistent with our observations of grain contact surfaces. The island-channel model may be more realistic in that it does not require the grain boundary fluid pressure to be elevated relative to the pore fluid. It is a different conceptual model, with different implications for the controls on calcite dissolution, but in other respects still leads to the same question about the relative roles of surface reaction and diffusion in controlling pressure solution creep.

6.6. Surface reaction versus diffusion-control

Our results suggest that there may be a significant role for reaction-controlled compaction in our experiments. It is instructive to evaluate whether this is to be expected based on our interpretation of the ZSP model, and how expectations would change if there were different reaction rates or diffusion limitations. One approach is to determine the critical grain size where dissolution- and diffusion-control strain rates should be equal, which can be calculated by equating the rate expressions in equations (9) and (10) and solving for the average grain size, *d*, as a function of p_{eff} and total strain (Fig. 13). This analysis applies to the thin-film model. The corresponding graph for the island-channel model would be similar but more complicated because of the additional parameter A_{asp}.

The calculated critical grain size has a minimum at σ_{eff} = 67 MPa and increases at both higher and lower stresses. The increase at low stress is due to the nonlinear kinetic formulation (n = 3) and may be exaggerated since there are experimental data suggesting that reaction order decreases to 1 or even less than 1 at small departures from equilibrium (Adkins et al., 2021). The field where diffusion-limited dissolution predominates expands with increasing strain. Reaction-control should predominate at small strains for grain size up to 10 μm, and in general for grain sizes < 3 μm. For the 80 to 160 μm grains in our experiments pressure solution could start in the reaction-controlled regime but should be diffusion controlled for strain > 1 %. Indeed, the predicted strain rates for diffusion-control are much slower than for reaction-control (Figs. 12, 13), but the measured strain rates in both experiments are higher than the predictions for diffusion-control. Two factors might expand the reaction-control regime substantially. Reaction rates are likely to be slower than equation (10) predicts, due to limitations in reactive surface area on the grain contract surfaces (A ≪ 1), and the DSC factor in equation (9) could be larger (deMeer et al., 2005) as depicted with the curve for DS=10^{-18} m^3/s. Both these factors are likely to apply for the island-channel model too.

6.7. Time-dependent surface reaction rates

In our experiments we measured strain rate and reaction rate concurrently, and although the strain rates predicted for reaction control are higher than the measured rates, the discrepancy is not so large at the beginning of the experiments. There is a possibility that the strain rates are reaction-controlled throughout the experiments and slow with time because *the dissolution rates slow with time*. In this scenario, the problem in modeling the strain rate is not in accounting for the change in geometry (and hence p_{eff}) with strain, but in predicting the time-dependence of dissolution rates. The observation that strain rates in our experiment are roughly inversely proportional to grain size is also consistent with a significant role for reaction-control (equation (10), although this conclusion should be mediated by the relatively wide range of grain sizes in our experiments.

The 1/t evolution of strain rate in both of our experiments, a behavior that is commonly observed (Zhang and Spiers, 2005a; Zhang et al., 2010), could be significant in the context of reaction rate variations in that it is not obviously expected from the ZSP geometric models. Equation (9) predicts that strain rates should decrease exponentially, and the prediction from equation (10) depends strongly on the departure from equilibrium and other factors. The island-channel model has the potential to match the observations, if for example the asperity population changes systematically with time and strain. Another possibility is that the 1/t rate evolution could be an indication that strain rates are reaction-controlled and that the reaction rates vary as 1/t, a possibility that is not accounted for in the existing theory but would be consistent with other observations of mineral-fluid reaction rates. For example, calcite dissolution rates in nature tend to be both slower than predicted from laboratory experiment-derived kinetic parameters, and to decrease with time roughly as 1/time (Zhang et al., 2023 and references therein) presumably due to processes that passivate the reacting calcite surface over time under otherwise constant conditions (e.g. Reeves and Rothman, 2013). This same dependence is inferred from natural weathering processes affecting silicates (White and Brantley, 2003).

7. Conclusions

The primary conclusion from the results of granular calcite compaction experiments and the use of geochemical data to determine the *in-situ* reaction rates, is that the reactions predicted from theory qualitatively track the mechanical compaction of our samples and occur at rates that are the right order of magnitude to account for strain. All three types of chemical data we use (Sr/Ca, Mg/Ca, $^{87}Sr/^{86}Sr$) yield comparable reaction rates that are generally consistent with the observed compaction if it is controlled by dissolution on mineral grain contact surfaces. The calculated reaction rates are within the range expected if the solubility of calcite along the grain contact surfaces is enhanced due to an effective pressure that is higher than the applied stress by factors of about 10 to 70, or by much higher stresses concentrated at asperities on grain contact surfaces. However, measured reaction rates decrease more quickly with time than is predicted by the grain contact stress evolution in the Zhang et al. (2010) model. The measured reaction rates, and the measured strain rates, decrease approximately as 1/time, which could result from an intrinsic time-dependence to the reaction rates as observed in other contexts involving calcite dissolution and precipitation, or as a consequence of asperities being systematically eliminated during compaction.

Our results demonstrate that the method of using trace element and isotope ratios to monitor *in-situ* reactions can be a powerful tool for deconvolving the relative roles of different deformation mechanisms, and to better understand the role of temperature, stress and chemical environment on the evolution of sediments. This tool will require further development and testing, but may also be applicable to more complicated systems such as polymineralic samples and more complex pore fluid compositions, as well as to assess the effects of reaction retardants such as Mg and SO_4, and expedients such as NaCl (e.g. Zhang and Spiers, 2005a). Our results also show that the structure of grain boundaries is central to understanding both the relative contributions of cracking and pressure solution and the rate-limiting step during pressure solution. More accurate flow laws would need to account better for the evolving structure of grain boundaries during chemical–mechanical deformation, as well for time-dependence of chemical reaction rates under otherwise constant or slowly evolving conditions.

CRediT authorship contribution statement

Harrison Lisabeth: Writing – review & editing, Writing – original draft, Formal analysis, Conceptualization. **Donald J. DePaolo:** Writing – review & editing, Writing – original draft, Formal analysis, Conceptualization. **Nicholas J. Pester:** Writing – original draft, Formal analysis, Conceptualization. **John N. Christensen:** Writing – review & editing, Writing – original draft, Formal analysis, Conceptualization.

Declaration of competing interest

The authors declare that they have no known competing financial interests or personal relationships that could have appeared to influence the work reported in this paper.

Acknowledgements

This research was supported by the U.S. Department of Energy, Office of Science, Office of Basic Energy Sciences, Chemical Sciences, Geosciences, and Biosciences Division, through its Geoscience program at LBNL under Contract DEAC02-05CH11231.

Appendix A. Supplementary material

Supplementary information is provided in four sections: Section 1 provides additional experimental details including on sample preparation, measurement procedures and precision, background on Sr and Mg distribution coefficients, pore pressure and permeability evolution during the experiments, and analysis of the effect of unequal dissolution and precipitation rates. Section 2 descibes the details of the model used to predict reaction rates from fluid chemistry. Section 3 describes the results of Experiment 2, carried out at Beamline 8.3.2 at the Advanced Light Source. Section 4 is a list of symbols, parameters, and formulae used in the manuscript. Supplementary material to this article can be found online at https://doi.org/10.1016/j.gca.2024.09.018.

References

Adkins, J.F., Naviaux, J.D., Subhas, A.V., Dong, S., Berelson, W.M., 2021. The dissolution rate of $CaCO_3$ in the ocean. Ann. Rev. Mar. Sci. 13, 57–80.
Atkinson, B.K., 1984. Subcritical crack growth in geological materials. J. Geophys. Res. 89 (B6), 4077–4114.
Baker, P., Kastner, M., Byerlee, J., Lockner, D., 1982. Pressure solution and hydrothermal recrystallization of carbonate sediments—an experimental study. Mar. Geol. 38 (1980), 185–203.
Brantut, N., Heap, M.J., Meredith, P.G., Baud, P., 2013. Time-dependent cracking and brittle creep in crustal rocks: a review. J. Struct. Geol. 52, 17–43.
Brantut, N., Heap, M., Baud, P., Meredith, P., 2014. Mechanisms of time dependent deformation in porous limestone. J. Geophys. Res. 119, 5444–5463.
Chanda, P., Gorski, C.A., Oakes, R.L., Fantle, M.S., 2019. Low temperature stable mineral recrystallization of foraminiferal tests and implications for the fidelity of geochemical proxies. Earth Planet. Sci. Lett. 506, 428–440.
Croize, D., Renard, F., Bjørlykke, K., Dysthe, D., 2010. Experimental calcite dissolution under stress: evolution of grain contact microstructure during pressure solution creep. J. Geophys. Res.-Solid Earth, 115.
Croizé, D., Renard, F., Gratier, J.-P., 2013. Chapter 3 - compaction and porosity reduction in carbonates: a review of observations, theory, and experiments. In: Dmowska, R. (Ed.), Adv. Geophys. (Vol. 54, pp. 181-238): Elsevier.
DeBoer, R.B., 1977. On the thermodynamics of pressure solution – interaction between chemical and mechanical forces. Geochim. Cosmochim. Acta 41, 249–256.
deMeer, S., Spiers, C.J., Nakashima, S., 2005. Structure and diffusive properties of fluid-filled grain boundaries: an in-situ study using infrared (micro) spectroscopy. Earth Planet. Sci. Lett. 232, 403–414.
Dong, S., Subhas, A.V., Rollins, N.E., Naviaux, J.D., Adkins, J.F., Berelson, W.M., 2018. A kinetic pressure effect on calcite dissolution in seawater. Geochim. Cosmochim. Acta 238, 411–423.
Heidug, W.K., 1991. A thermodynamic analysis of the conditions of equilibrium at nonhydrostatically stressed and curved solid-fluid interfaces. J. Geophys. Res. Solid Earth 96 (B13), 21909–21921.
Hickman, S.H., Evans, B., 1995. Kinetics of pressure solution at halite-silica interfaces and intergranular clay films. J. Geophys. Res. 100 (B7), 13113–13132.
Jonasson, R.G., Rispler, K., Wiwchar, B., Gunter, W.D., 1996. Effect of phosphonate inhibitors on calcite nucleation kinetics as a function of temperature using light scattering in an autoclave. Chem. Geol. 132 (1–4), 215–225.
Le Guen, Y., Renard, F., Hellmann, R., Brosse, E., Collombet, M., Tisserand, D., Gratier, J. P., 2007. Enhanced deformation of limestone and sandstone in the presence of high fluids. J. Geophys. Res. Solid Earth 112 (B5).
Lehner, F.K., 1995. A model for intergranular pressure solution in open systems. Tectonophysics 245, 153–170.
Lehner, F.K., 1990. Thermal dynamics of rock deformation by pressure solution. In: Deformation Processes in Minerals, Ceramics and Rocks, edited by D. J. Barber and P. G. Meredith, pp. 296–333, Unwin Hyman, London.
Lisabeth, H.P., Zhu, W., 2015. Effect of temperature and pore fluid on the strength of porous limestone. J. Geophys. Res. Solid Earth 120 (9), 6191–6208.
Liteanu, E., Spiers, C.J., 2009. Influence of pore fluid salt content on compaction creep of calcite aggregates in the presence of supercritical CO2. Chem. Geol. 265 (1–2), 134–147.
McDonald, R.W., North, N.A., 1974. The effect of pressure on the solubility of $CaCO_3$, CaF_2, and $SrSO_4$ in water. Can. J. Chem. 52, 3181–3186.
Mucci, A., Morse, J.W., 1983. The incorporation of Mg2+ and Sr2+ into calcite overgrowths: influences of growth rate and solution composition. Geochimica Cosmochimica Acta 47, 217–233.
Palandri, J., 2015. SOLTHERM Thermodynamic Database for Geochemical Modeling. United States: N.p., 07 Oct, 2015.
Reeves, D., Rothman, D.H., 2013. Age dependence of mineral dissolution and precipitation rates. Global Biogeochem. Cycles 27 (3), 906–919.
Renard, F., Dysthe, D., Feder, J., Bjørlykke, K., Jamtveit, B., 2001. Enhanced pressure solution creep rates induced by clay particles: experimental evidence in salt aggregates. Geophys. Res. Lett. 28 (7), 1295–1298.
Rutter, E., 1983. Pressure solution in nature, theory and experiment. J. Geol. Soc. London 140, 725–740.
Scholle, P.A., Halley, Robert B., 1985. Burial diagenesis: out of sight, out of mind!, Carbonate Cements: Based on a Symposium Sponsored by the Society of Economic Paleontologists and Mineralogists, Nahum Schneidermann, Paul M. Harris.
Snieder, R., Sens-Schonelder, C., Wu, R., 2017. The time dependence of rock healing as a universal relaxation process, a tutorial. Geophys. J. Int. 208, 1–9.
Spiers, C.J., Schutjens, P.M.T.M., 1990. Densification of crystalline aggregates by fluid-phase diffusional creep. In: Barber, D.J., Meredith, P.G. (Eds.), Deformation Processes in Minerals, Ceramics and Rocks. Unwin Hyman, London, pp. 334–353.

Spiers, C.J., Schutjens, P.M.T.M., Brzesowsky, R.H., Peach, C.J., Liezenberg, J.L., Zwart, H.J., 1990. Experimental determination of constitutive parameters governing creep of rocksalt by pressure solutionDeformation Mechanisms, Rheology and Tectonics, edited by R. J. Knipe and E. H. Rutter. Geol. Soc. Spec. Publ. 54, 215–227.

Vajdova, et al., 2010. Micromechanics of inelastic compaction in two allochemical limestones. J. Struct. Geol. 43.

Voltolini, M., Haboub, A., Dou, S., Kwon, T.-H., MacDowell, A.A., Parkinson, D.Y., Ajo-Franklin, J., 2017. The emerging role of 4D synchrotron X-ray micro-tomography for climate and fossil energy studies: five experiments showing the present capabilities at beamline 8.3.2 at the advanced light source. J. Synchrotron Radiat. 24 (6), 1237–1249.

Weyl, P.K., 1959. Pressure solution and the force of crystallization: a phenomenological theory. J. Geophys. Res. 64 (11), 2001–2025.

White, A.F., Brantley, S.L., 2003. The effect of time on the weathering of silicate minerals: Why do weathering rates differ in the laboratory and field? Chem. Geol. 202, 479–506.

Zhang, S., DePaolo, D.J., Huang, Y., Wang, G., 2023. Origin and significance of ultra-slow calcite dissolution rates in deep sea sediments. Geochim. Cosmochim. Acta in press.

Zhang, X., Salemans, J., Peach, C.J., Spiers, C.J., 2002. Compaction experiments on wet calcite powder at room temperature: Evidence for operation of intergranular pressure solution. Geological Society, London, Special Publications 200 (1), 29–39.

Zhang, X., Spiers, C.J., 2005a. Compaction of granular calcite by pressure solution at room temperature and effects of pore fluid chemistry. Int. J. Rock Mech. Min. Sci. 42 (7–8), 950–960.

Zhang, X., Spiers, C.J., 2005b. Effects of phosphate ions on intergranular pressure solution in calcite: an experimental study. Geochim. Cosmochim. Acta 69 (24), 5681–5691.

Zhang, X., Spiers, C.J., Peach, C.J., 2010. Compaction creep of wet granular calcite by pressure solution at 28 C to 150 C. J. Geophys. Res. Solid Earth 115 (B9).

Zhu, W., Baud, P., Wong, T.-F., 2010. Micromechanics of cataclastic pore collapse in limestone. J. Geophys. Res. 115, B04405.